Int. J. Heat Mass Transfer. Vol. 27, No. 11, pp. 2133–2144, 1984
Printed in Great Britain

0017-9310/84 $3.00 + 0.00
Pergamon Press Ltd.

Symmetric vs asymmetric periodic disturbances at the walls of a heated flow passage

E. M. SPARROW and W. Q. TAO

Department of Mechanical Engineering, University of Minnesota, Minneapolis, MN 55455, U.S.A.

(*Received* 23 *December* 1983 *and in revised form* 7 *March* 1984)

Abstract—Measurements were made of local and fully developed turbulent heat transfer coefficients for a flat rectangular duct having streamwise-periodic, two-dimensional disturbances symmetrically positioned at both principal walls. Friction factors were also determined. The local transfer coefficient distributions revealed the rapid attainment of the periodic fully developed regime. The fully developed transfer coefficients exceeded (typically by 40%) those for an otherwise identical duct having periodic disturbances at only one of the principal walls (asymmetric case). The symmetric disturbances also yielded significantly increased transfer coefficients (up to a factor of three) compared with a corresponding disturbance-free duct. Large disturbance-related increases in the friction factor were also sustained. An analysis based on fixed duct dimensions and fixed pumping power was made to assess the relative performance of the symmetrically and asymmetrically disturbed ducts and the disturbance-free duct. For a wide range of conditions, the symmetrically disturbed duct yielded the highest fully developed transfer coefficients. Compact correlations in terms of roughness parameters were developed for both the fully developed heat transfer coefficients and friction factors.

INTRODUCTION

THE RESEARCH described here is the second and concluding part of an in-depth, two-part experimental study of streamwise-periodically-disturbed turbulent heat transfer and pressure drop in a flat rectangular duct. The work was motivated by the search for enhancement techniques for heat transfer in the flow passages of heat exchange devices.

In the first part of the study [1], two-dimensional disturbance elements were periodically deployed adjacent to one of the principal walls of the duct. Each disturbance element was a small-diameter circular rod which was oriented transverse to the flow direction and which spanned the full width of the duct. The other principal wall of the duct was smooth (i.e. free of disturbance elements). Two geometrical parameters were varied during the course of the experiments including: (1) the ratio of the streamwise pitch of the disturbance elements to the element height (i.e. diameter) and (2) the ratio of the disturbance element height to the duct height. For each configuration, the duct Reynolds number was varied between 10 000 and 45 000. In addition, two thermal boundary conditions were investigated: (1) the same uniform temperature at both principal walls and (2) uniform temperature at the wall adjacent to the disturbance elements; no heat transfer at the smooth principal wall.

Local heat transfer coefficients were measured at 160 axial stations, and this information was employed to determine cycle-averaged, fully developed heat transfer coefficients. The fully developed coefficients at the disturbance-adjacent wall were enhanced by as much as 140% compared with those for the corresponding smooth-walled duct. For the average coefficient encompassing both principal walls (both at uniform wall temperature), enhancements as large as 90% were encountered. The measured fully developed friction factors were several times larger than those for the smooth duct. Both the fully developed heat transfer coefficients and friction factors were successfully correlated using roughness parameters.

The research reported here was undertaken to fulfill two objectives. The first was to extend the previous work [1] to the case in which there are disturbance rods positioned adjacent to *both* of the principal walls of the duct. For this case, the same geometrical and flow parameters will be employed and varied as in ref. [1] for the one-sided disturbed duct. For these experiments, both of the principal walls are maintained at the same uniform temperature. The experiments yield local heat transfer coefficients, cycle-averaged, fully developed heat transfer coefficients, and fully developed friction factors. Correlations of the fully developed results will be developed in terms of roughness parameters.

The second objective of the work was to quantify the performance of both the one- and two-sided disturbed ducts with respect to a corresponding smooth-walled duct. In order to take account of both the heat transfer and pressure drop characteristics of the various ducts, the comparison will be made for the condition of equal pumping power. The outcome of the comparison will be a rank ordering of the one-sided disturbed duct, the two-sided disturbed duct, and the smooth-walled duct based on which yields the highest heat transfer coefficient for a given pumping power.

The smooth-walled heat transfer and pressure drop data needed for the aforementioned performance appraisal were measured in ref. [1] and were found to be in excellent agreement with available literature information. The literature survey set forth in ref. [1] for duct flows with wall-adjacent periodic disturbances

NOMENCLATURE

A_{cyc}	mass transfer area, pW
AR	aspect ratio, W/H
D_h	hydraulic diameter
$\mathscr{D}$	diffusion coefficient
e	disturbance height (rod diameter)
e^+	roughness Reynolds number, equation (12)
f	fully developed friction factor
H	duct height
H_e^+	heat (mass) transfer function, equation (13)
h_{fd}	cycle-averaged, fully developed heat transfer coefficient
h_{fd}^*	fully developed heat transfer coefficient for disturbance-free duct
$K(X)$	local mass transfer coefficient
$\bar{K}_{cyc}$	cycle-averaged, fully developed mass transfer coefficient
K_{fd}	alternate designation for $\bar{K}_{cyc}$
K_{fd}^*	fully developed mass transfer coefficient for disturbance-free duct
$\dot{M}_{cyc}$	per-cycle fully developed mass transfer rate
$\dot{m}(X)$	local rate of mass transfer per unit area
P	pressure
PP	pumping power
p	center-to-center pitch of disturbance rods
R^+	modified roughness function, equation (11)
R_e^+	roughness function, equation (10)
Re	Reynolds number
Re^*	Reynolds number for disturbance-free duct
Sc	Schmidt number
$Sh(X)$	local Sherwood number
$\overline{Sh}_{cyc}$	cycle-averaged, fully developed Sherwood number
St	Stanton number
V	mean velocity
W	duct width
$\dot{w}$	mass flow rate through duct
X	axial coordinate.

Greek symbols

μ	viscosity
ν	kinematic viscosity
ρ	air density
ρ_{nb}	bulk density of naphthalene vapor
ρ_{nw}	density of naphthalene vapor at wall
$\Delta\rho_{cyc}$	per-cycle difference between ρ_{nw} and ρ_{nb}.

Superscript

*	disturbance-free duct.

is also applicable for the present investigation and needs no elaboration.

THE EXPERIMENTS

A schematic side view of the flat rectangular duct used in the experiments is presented in Fig. 1. The diagram shows the two principal walls of the duct and the circular-rod disturbance elements deployed adjacent to each of the walls. The two sets of rods are positioned at common axial stations, with the axial separation distance between the centers of successive rods denoted by p (pitch). Since p is uniform along the duct, the rods provide streamwise-periodic, two-dimensional disturbances.

In addition to the pitch p, the other two lengths which characterize the flow passage geometry are indicated in the figure—the height, H, of the duct and the height, e, of the disturbance elements (equal to the rod diameter). In non-dimensional terms, the passage geometry may be characterized by two dimension ratios involving the quantities p, H, and e. The ratios to be employed here are p/e and e/H, and Table 1 lists the investigated numerical values of these quantities. As seen there, for each of two disturbance height–duct height ratios, three values of the pitch–height ratio of the disturbance elements were employed. These parameter values were obtained by using ducts of two different heights (0.636 and 1.275 cm) and disturbance elements with three different pitches (0.952, 1.905, and 3.811 cm), while maintaining a fixed disturbance height (e = 1.051 mm). All told, then, six different configurations were investigated.

Another dimension ratio of potential relevance is the

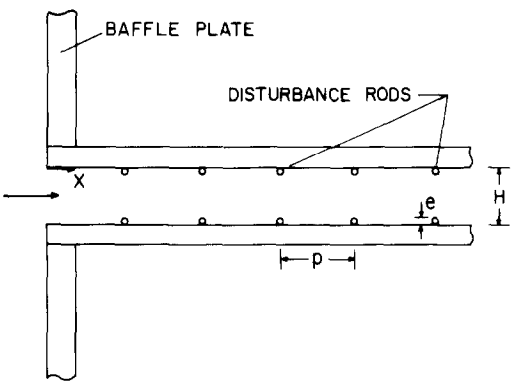

FIG. 1. Schematic side view of the duct test section with the disturbance elements in place.

Table 1. Flow passage characteristics

Case	e/H	AR	p/e
1	0.082	6.4	9.15
2			18.3
3			36.6
4	0.164	12.8	9.15
5			18.3
6			36.6

aspect ratio, $AR = W/H$ (where W is the width of the duct), of the duct cross-section. However, the values of AR employed in the experiments, 6.4 and 12.8, are believed to be sufficiently large to eliminate it as a significant parameter. By incorporating the aspect ratio into the conventional definition of the duct hydraulic diameter, D_h, it readily follows that $e/D_h = \frac{1}{2}(e/H)(1 + 1/AR)$, yielding an alternative measure of the relative height of the disturbance elements.

The disturbance rods spanned the entire width W of the duct. To hold the rods in place, holes had been drilled along the upper and lower edges of the duct side walls, and the rod ends were seated in these holes. The rods were cut from lengths of 1.051 mm diameter drill-rod stock, selected for straightness and uniformity of diameter.

Figure 1 also shows the inlet configuration of the duct. As seen there, the inlet is sharp edged. In addition, the upstream end of the duct is set into a large baffle plate. This arragement simulates the situation in which the duct inlet is built into the downstream wall of a large plenum chamber. At the downstream end of the duct (not shown), there is a rectangular-to-circular transition section which, in turn, is connected to an air handling system consisting of a flow meter, a control valve, and a blower.

The system is operated in the suction mode, with air from the temperature-controlled laboratory being drawn into the duct inlet. The blower is located in an adjacent room, and the blower discharge is vented outside the building.

The naphthalene sublimation technique was used in the execution of the experiments because it affords several advantages compared with direct heat transfer measurements. By employing the well-established analogy between heat and mass transfer, the mass transfer coefficients and Sherwood numbers determined here can be transformed to heat transfer coefficients and Nusselt numbers.

The surface of each principal wall was of naphthalene, freshly cast for each data run. The surface finish of the naphthalene was comparable to that of the highly polished stainless steel plate against which the casting was made. The side walls of the duct were metallic (aluminum) and, therefore, did not participate in the mass transfer process.

At the principal walls, the mass transfer boundary condition was that the density of the naphthalene vapor is uniform. By the analogy, this corresponds to uniform wall temperature in the corresponding heat transfer problem. The mass transfer inactive side walls correspond to adiabatic surfaces.

The naphthalene vapor density in equilibrium with a solid naphthalene surface depends on the surface temperature. Since the vapor density at the principal walls of the duct is needed in the data reduction, the surface temperature was measured by calibrated thermocouples that were embedded in the solid during the casting process. Two thermocouples were installed in each wall. Deviations among the thermocouple readings were never greater than 0.05–0.1°C.

The local mass transfer coefficients were deduced from measurements of the surface contours of the principal walls. Such measurements were performed both before and after each data run. By differencing the before and after measurements, the amount of mass sublimed at each measurement station was determined. At each principal wall, the surface contour was measured in a 160-point axial traverse along each of three parallel lines, one of which was situated midway between the duct side walls while the others were respectively situated to either side of the midline, halfway between it and the side wall. The measurement system (depth sensor and electronics) had a resolving power of 10^{-5} in. Further details of the surface contour measurements are given in ref. [1].

Pressure drop experiments were performed using an auxiliary apparatus in which the naphthalene-surfaced principal walls were replaced by metallic walls. The axial deployment of the pressure taps was tailored to take account of the streamwise periodic nature of the flow. In particular, in the periodic fully developed regime, the pressure drop per cycle (i.e. in an axial length p) is a constant. Consequently, pressure taps with an axial spacing p (or an integer multiple of p) will yield a linear pressure distribution in the fully developed regime. This pressure tap pattern was adopted in the experiments. Pressure drops were measured with a capacitance-type, solid-state pressure meter capable of resolving 10^{-3} or 10^{-4} Torr, depending on the pressure level.

DATA REDUCTION

Two types of mass transfer coefficients (and corresponding Sherwood numbers) were evaluated from the experimental data. One of these is the local transfer coefficient at any axial station X. The other is the cycle-averaged transfer coefficient for the periodic fully developed regime.

For the evaluation of the local coefficient, the first step is to average out any slight differences in the sublimation rates at a given X among the three parallel lines along which the contour measurements were made at each principal wall. Furthermore, the two principal walls yielded virtually the same local mass

transfer rates, and any small differences were averaged out. Then, let $\dot{m}(X)$ denote the local rate of mass transfer per unit area at X. Also, let ρ_{nw} denote the naphthalene vapor density at the principal walls and $\rho_{nb}(X)$ the bulk naphthalene vapor density at X. With these, the local mass transfer coefficient $K(X)$ is

$$K(X) = \dot{m}(X)/[\rho_{nw} - \rho_{nb}(X)]. \quad (1)$$

Among the quantities appearing in equation (1), $\dot{m}(X)$ is determined directly from the differences between the surface contours measured before and after the data run (equation (2) of ref. [1]). The density ρ_{nw} is evaluated from the vapor pressure–temperature relation for naphthalene in conjunction with the perfect gas law (note that ρ_{nw} is independent of X). For $\rho_{nb}(X)$, the naphthalene subliming from the walls between $X = 0$ and X is balanced by the increase in the naphthalene vapor content of the air between those stations (equation (5) of ref. [1]; note also that $\rho_{nb} = 0$ at $X = 0$).

Attention will next be turned to the cycle-averaged, fully developed mass transfer coefficient. As a first step, the per-cycle, fully developed mass transfer rate $\dot{M}_{cyc}$ is evaluated from

$$\dot{M}_{cyc} = \int_{x}^{x+p} \dot{m}(X) W \, dX \quad (2)$$

where X and $(X + p)$ are situated in the fully developed regime. Since $\dot{m}(X)$ is already averaged for the two principal walls, the individual walls need not be considered separately. The mass transfer surface area corresponding to $\dot{M}_{cyc}$ is $A_{cyc} = pW$.

The per-cycle mass transfer is driven by the mean per-cycle difference between ρ_{nw} and ρ_{nb}. This difference, to be denoted by $\Delta\rho_{cyc}$, involves $\rho_{nb}(X)$ and $\rho_{nb}(X+p)$, as well as ρ_{nw}. These quantities were individually evaluated as described in the foregoing. For $\Delta\rho_{cyc}$, calculations were made for three different models: (1) log mean, (2) arithmetic mean, and (3) integrated mean of $[\rho_{nw} - \rho_{nb}(X)]$. The mass transfer coefficients based on these calculation models were identical within plotting accuracy.

In terms of the quantities defined in the preceding paragraphs

$$\bar{K}_{cyc} = \dot{M}_{cyc}/A_{cyc}\Delta\rho_{cyc}. \quad (3)$$

The dimensionless counterparts of $K(X)$ and $\bar{K}_{cyc}$ are the Sherwood numbers

$$Sh(X) = K(X)D_h/\mathscr{D}, \quad \overline{Sh}_{cyc} = \bar{K}_{cyc}D_h/\mathscr{D} \quad (4)$$

in which D_h is the conventional hydraulic diameter $[2HW/(H+W)]$, and $\mathscr{D}$ is the naphthalene–air diffusion coefficient. The latter is eliminated by using the Schmidt number Sc, which gives

$$1/\mathscr{D} = (1/\nu)Sc \quad (5)$$

and $Sc = 2.5$ for the naphthalene–air system.

The pressure drop and friction factor will now be considered. As noted earlier, the pressure taps were positioned to measure the per-cycle pressure drop in the fully developed regime, which is the same from cycle to cycle. From the resulting linear pressure distribution, the gradient dP/dX was determined and used in the evaluation of the fully developed friction factor

$$f = (-dP/dX)D_h/\tfrac{1}{2}\rho V^2 \quad (6)$$

where $\rho V^2 = (\dot{w}/HW)^2/\rho$, in which $\dot{w}$ is the mass flow rate and ρ is the density in the fully developed regime.

The Reynolds number was employed as a dimensionless representation of the mass flow

$$Re = \rho V D_h/\mu = 2\dot{w}/\mu(H+W). \quad (7)$$

Re was evaluated from the rightmost term of equation (7).

DISTRIBUTIONS OF THE LOCAL MASS TRANSFER COEFFICIENT

Each data run yielded the axial distribution of the local Sherwood number $Sh(X)$. A sampling of this information will now be presented. This presentation will complement the $Sh(X)$ distributions at the disturbance-adjacent wall for a one-sided disturbed duct as displayed in Figs. 2–6 of ref. [1].

As was noted earlier, the mass transfer results for the two principal walls were virtually identical, and whatever small differences did exist were averaged out. The $Sh(X)$ distributions now to be presented are, therefore, representative of both walls.

Figure 2 displays the response of the local Sherwood number distribution to changes in Reynolds number.

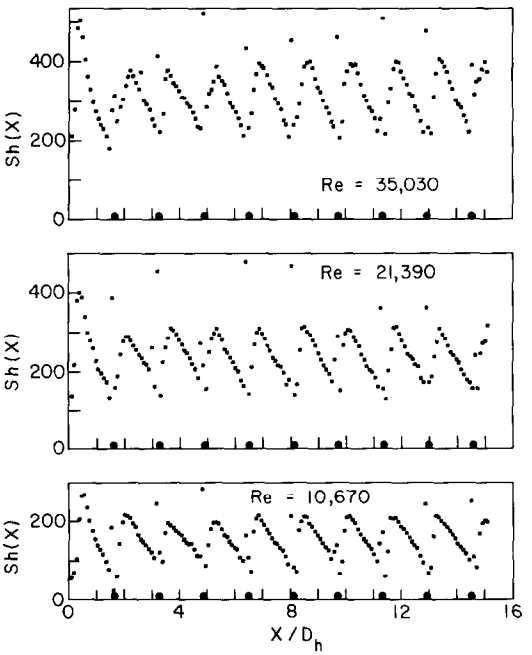

FIG. 2. Response of the local Sherwood number distribution to changes in Reynolds number ($e/H = 0.164$, $p/e = 18.3$).

In the figure, $Sh(X)$ is plotted as a function of X/D_h for $Re = 10\,700$, $21\,400$, and $35\,000$. These results correspond to fixed values of the geometric parameters e/H and p/e, respectively equal to 0.164 and 18.3. Along the abscissa of each graph in Fig. 2 are black circles which indicate the axial positions of the disturbance rods.

Before considering the effect of Reynolds number, it is appropriate to comment on the general character of the $Sh(X)$ distributions. The portion of the distribution upstream of the first rod reflects the separation of the flow at the sharp-edged inlet of the duct. In particular, the first peak corresponds to the reattachment of the separated flow. The remainder of the $Sh(X)$ distribution is shaped and controlled by the presence of the periodic disturbances. It is seen that $Sh(X)$ takes on a periodic pattern almost immediately, and the virtual absence of an entrance region is noteworthy.

The flow separates each time it encounters a disturbance rod. Reattachment occurs in the inter-rod space, and each reattachment corresponds to a peak in the $Sh(X)$ distribution. Subsequent to reattachment, the flow begins to redevelop, causing $Sh(X)$ to drop off. The dropoff is arrested as the flow encounters the next disturbance rod, and $Sh(X)$ increases as the separated flow approaches reattachment.

At axial stations in the neighborhood of the disturbance rods, there are occasional data points which do not fall on the mainline $Sh(X)$ distribution. These points, which, for the most part, are high, are not scatter. Rather, they reflect the presence of intense, compact vortices situated immediately upstream and downstream of the disturbance rod.

With regard to the Reynolds number, its main effect is to change the level of the $Sh(X)$ distribution. However, the shape of the distribution is virtually unaffected. In particular, the location at which the maximum occurs (i.e. the point of flow reattachment in the inter-rod space) is unchanged in the investigated Reynolds number range. There is, however, a tendency for the maximum to become somewhat more peaked with increasing Reynolds number. This peaking tendency is associated with a more rapid dropoff of $Sh(X)$ downstream of the maximum.

The next issue to be considered is the effect of the pitch p of the disturbance rods on the $Sh(X)$ distribution, and Fig. 3 has been prepared for this purpose. Results are given for $p/e = 9.15$, 18.3, and 36.6 for fixed values of $Re = 12\,700$ and $e/H = 0.082$. In considering this figure, it is helpful to take note of the black circles along the abscissa of each graph which serve to depict the positions of the disturbance rods.

Inspection of Fig. 3 shows that the main effect of a change in pitch is to alter the extent of the flow redevelopment which follows reattachment. With increasing pitch (i.e. larger inter-rod space), the amount of redevelopment increases. This is especially evident in the results for $p/e = 36.6$, where the flattening of the $Sh(X)$ distribution in the aft portion of the inter-rod space testifies to the considerable amount of redevelopment that has occurred. Thus, the velocity

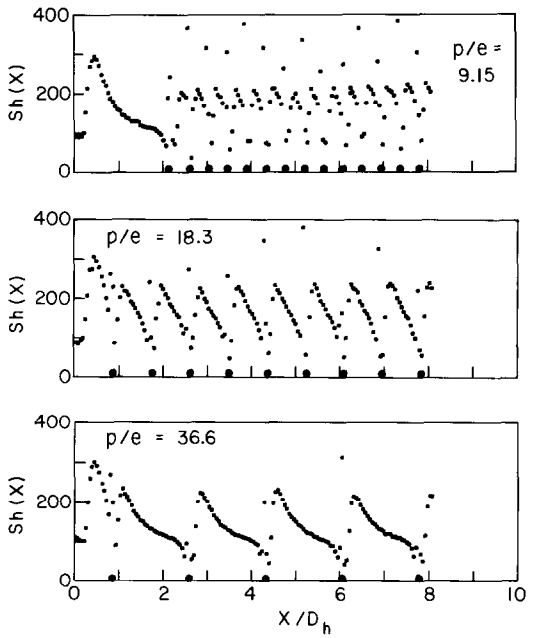

FIG. 3. Response of the local Sherwood number distribution to changes in pitch ($Re = 12\,700$, $e/H = 0.082$).

distribution in the flow approaching the next disturbance rod (which is directly related to the degree of redevelopment of the flow) changes as the pitch changes. Despite this, the distance downstream of the rod at which reattachment occurs is virtually unaffacted by changes in pitch.

The final aspect of the $Sh(X)$ distributions to be considered is the effect of the relative heights of the disturbance rods and the duct. Figure 4 shows results

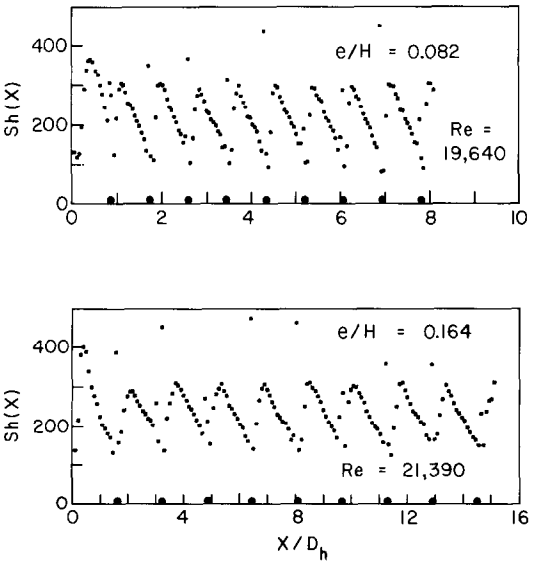

FIG. 4. Response of the local Sherwood number distribution to changes in the relative heights of the disturbance rods and the duct ($Re \simeq 20\,000$, $p/e = 18.3$).

for $e/H = 0.082$ and 0.164 for $Re \simeq 20000$ and $p/e = 18.3$. Note that the X/D_h scales for the two graphs are different because of the different D_h values for the two cases. The shapes of the two $Sh(X)$ distributions are the same. Indeed, if not for the different abscissa scales, they would be very nearly coincident, aside from the non-mainline points, which tend to be irregular. Also, the distribution for $e/H = 0.082$ appears to bottom-out at slightly lower values than does the $e/H = 0.164$ distribution.

FULLY DEVELOPED MASS TRANSFER AND FRICTION RESULTS

As noted earlier, the per-cycle mass transfer coefficient and Sherwood number are constant in the periodic fully developed regime. In addition, the constancy of the per-cycle pressure drop enables a fully developed friction factor to be defined and evaluated. The fully developed regime is of particular importance in periodically disturbed flows because the entrance length is very short (Figs. 2–4).

Sherwood numbers

The per-cycle fully developed Sherwood numbers are plotted in Fig. 5 as a function of the Reynolds number. The figure conveys results for all six of the investigated configurations. In order to avoid overlap, the results for $e/H = 0.164$ are plotted as $2\overline{Sh}_{cyc}$, while those for $e/H = 0.082$ are plotted directly as $\overline{Sh}_{cyc}$. Within each e/H grouping, the p/e parameter is assigned values of 9.15, 18.3, and 36.6.

The straight lines which pass through the data are least-squares fits of the form

$$\overline{Sh}_{cyc} = C\,Re^n \tag{8}$$

where the constants C and n are listed in Table 2. The exponents n (slopes of the lines in Fig. 5) are clustered in the range 0.59–0.65. The n values are very slightly higher for $e/H = 0.082$ (cases 1–3) than for $e/H = 0.164$ (cases 4–6), but there is no systematic variation with p/e. There is virtually no scatter of the data points relative to the least-squares lines.

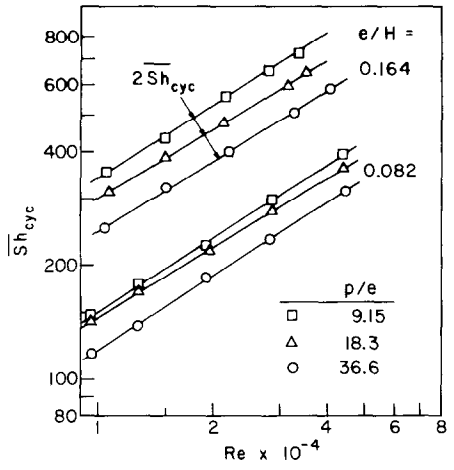

FIG. 5. Per-cycle fully developed Sherwood numbers.

The figure shows that for fixed values of the other parameters, more closely spaced disturbance elements (smaller p/e) give rise to higher Sherwood numbers. It may also be observed that the duct with the lesser height ($e/H = 0.164$) is more responsive to changes in p/e than is the duct with the greater height ($e/H = 0.082$).

After taking account of the two-fold scaling, it can be verified that the $p/e = 36.6$ curves for the two e/H values are virtually coincident and that the $p/e = 18.3$ curves deviate from each other by only a few percent. For $p/e = 9.15$, the deviation between the two curves is in the 10% range. Therefore, for fixed values of Re and p/e, the Sherwood number is not very sensitive to e/H. However, it does not necessarily follow that the mass transfer coefficient is similarly insensitive to e/H. This is because a H-related difference in e/H may give rise to different values of D_h, which have to be used when the mass transfer coefficient is extracted from the Sherwood number.

The per-cycle fully developed Sherwood numbers just presented for the two-sided disturbed duct will now be compared with those for the one-sided disturbed duct that was investigated in ref. [1]. The comparison is displayed in Figs. 6 and 7, which correspond to fixed values of $e/H = 0.082$ and 0.164, respectively. The lines appearing in these figures are least-squares fits of the experimental data (the actual data are displayed in Fig. 5 and in Figs. 8 and 9 of ref. [1]).

In each figure, the results are grouped according to p/e. In each grouping, there are three lines. One of these is for the two-sided disturbed duct (two rodded walls), while the others are for the one-sided disturbed duct (one rodded/one smooth). Note that for the latter duct, both the rodded and smooth walls participate in the mass transfer process. For this duct, Sherwood number results are shown separately for the rodded wall and for the average of the smooth and rodded walls.

From an overall inspection of Figs. 6 and 7, it is seen that the per-cycle fully developed Sherwood numbers for a two-sided disturbed duct always exceed those for a one-sided disturbed duct. For concreteness, the smooth wall/rodded wall average for the one-sided case will be compared with the two-sided case. Such a comparison shows that relative to the one-sided disturbances, the two-sided disturbances give rise to Sherwood number enhancements in the 25–60% range, with 40% representing a typical enhancement.

In general, there is a tendency toward larger double-disturbance-related enhancements at lower Reynolds numbers, except at the smallest pitch ($p/e = 9.15$) where the enhancement is virtually independent of Reynolds number. Also, among the various disturbance pitches, the smallest enhancement occurs for the largest pitch. Globally speaking, the enhancements are not strongly dependent on e/H.

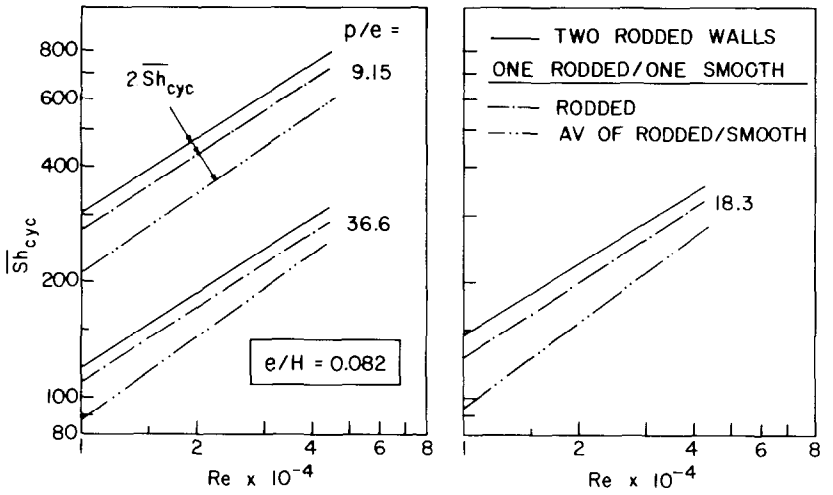

FIG. 6. Comparison of per-cycle fully developed Sherwood numbers for one- and two-sided disturbed ducts, $e/H = 0.082$.

Figures 5–7 have focused on the Sherwood numbers for ducts with periodic disturbances. To provide perspective for these results, the fully developed Sherwood numbers for corresponding disturbance-free ducts have been measured [1]. For $Re = 10, 20, 30$, and 40×10^3, the Sh values are 56.8, 96.4, 134, and 169. When these values are compared with those of Figs. 5–7, it is seen that the presence of the disturbance rods yields up to a three-fold increase in the Sherwood number at $Re = 10\,000$ and up to a 2.4-fold increase at $Re = 40\,000$. These impressive enhancements are accompanied by large increases in pressure drop, as will be demonstrated shortly. The trade-off between the higher Sherwood numbers and higher friction factors will be assessed later in the paper.

Friction factors

The fully developed friction factors are plotted in Fig. 8 as a function of the Reynolds number. The presentation includes both the one-sided disturbed duct and the two-sided disturbed duct. Data points are shown only for the latter since the data for the former are displayed in Fig. 7 of ref. [1]. The straight lines appearing in the figure are least-squares correlations of the form

$$f = C_1 Re^{-m}. \tag{9}$$

The constants C_1 and m for the two-sided disturbed duct are listed in Table 2, while those for the one-sided disturbed duct are given in ref. [1] in the text following equation (16).

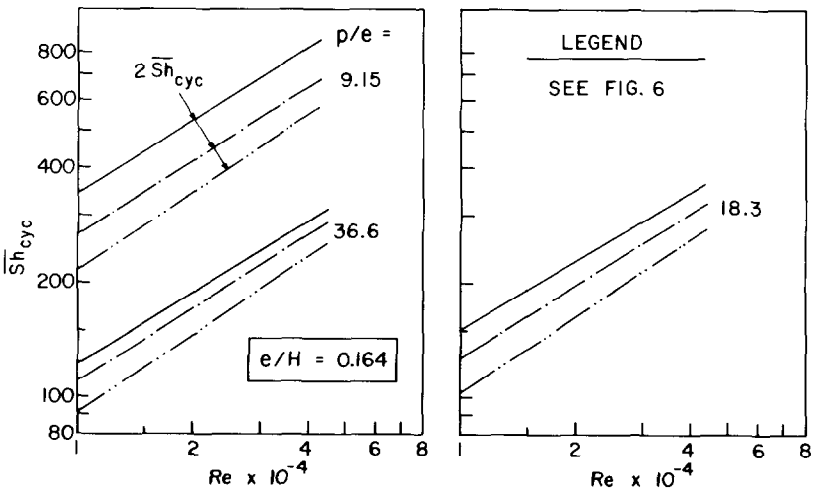

FIG. 7. Comparison of per-cycle fully developed Sherwood numbers for one- and two-sided disturbed ducts, $e/H = 0.164$.

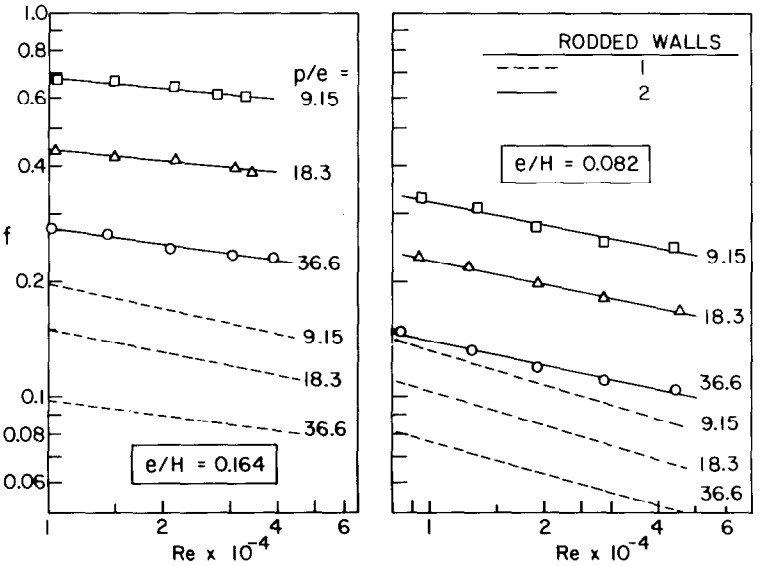

FIG. 8. Fully developed friction factors.

For the corresponding ducts without disturbances, the measured friction factors [1] are 0.0343, 0.0283, 0.0256, and 0.0239, respectively, for $Re = 10, 20, 30$, and 40×10^3.

From Fig. 8, it is seen that, as expected, the presence of disturbance rods at both principal walls takes a greater toll in pressure drop than do rods at one principal wall. The increase is, however, much greater for ducts of smaller height, as is seen by comparing the results for $e/H = 0.164$ with those for $e/H = 0.082$. This finding is physically plausible and is related to the appreciable blockage of the flow cross-section which occurs when disturbance elements are situated at both principal walls in a duct of relatively low height. In the present experiments, for the $e/H = 0.164$ configuration, the cross-sectional blockage was 32.8% at the axial stations at which the rods were situated. The greater pressure drop for the lower-height, two-sided disturbed duct will figure prominently in the performance evaluations to be presented later.

Another interesting point, evident both in Fig. 8 and in Table 2 for the two-sided disturbed duct, is that the f, Re curves for $e/H = 0.164$ are flatter than those for $e/H = 0.082$. It is well established that the flatter the f, Re distribution, the more significant are inertial losses relative to friction losses. Since greater cross-sectional blockage accentuates inertial losses, the flatter f, Re distributions for the $e/H = 0.164$ case are physically reasonable. As expected, the friction factor is larger for more closely spaced disturbances (i.e. for smaller p/e).

Table 2. Constants in equations (8) and (9)

Case	C	n	C_1	m
1	0.4056	0.6428	2.034	0.2003
2	0.5168	0.6126	1.588	0.2106
3	0.3092	0.6468	0.981	0.2113
4	0.5511	0.6229	1.682	0.0979
5	0.6275	0.5953	1.174	0.1062
6	0.4143	0.6178	0.982	0.1385

By comparing the f values of Fig. 8 with those indicated earlier for disturbance-free ducts, it is seen that the disturbance elements give rise to very large increases in pressure drop. Owing to the large parameter-dependent spread of the data, the extent of the increase is also highly parameter dependent, but factors of 5–10 fall within the observed range.

Correlations based on roughness parameters

A very compact presentation of the fully developed mass transfer and pressure drop results can be achieved in terms of the so-called roughness parameters. These parameters have already been used in ref. [1] to correlate the results for one-sided disturbed ducts, and they will be employed here (with selective modifications) for two-sided disturbed ducts.

The first step is to write the roughness function R_e^+ as set forth in ref. [1]

$$R_e^+ = (8/f)^{1/2} + 2.5 \ln (2e/D_h) + 4.23. \quad (10)$$

Next, a modified roughness function R^+ appropriate to the present two-sided disturbed ducts is introduced

$$R^+ = [(e/D_h)/(p/e)]^{0.4} R_e^+. \quad (11)$$

The Reynolds number is incorporated in another roughness parameter, e^+

$$e^+ = (f/8)^{1/2} (e/D_h) Re. \quad (12)$$

The friction factor, Reynolds number data for all of the two-sided disturbed cases were recast into the R^+, e^+ parameters and plotted in Fig. 9. The correlation of the data is seen to be very good, especially when account is taken of the large spread of the same data

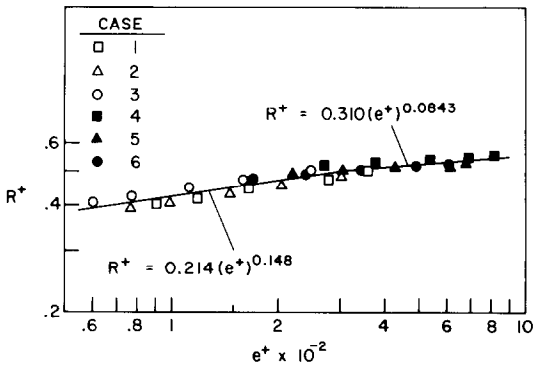

FIG. 9. Friction factor correlation in terms of roughness parameters.

when presented in terms of f and Re (see Fig. 8). Least-squares, straight-line correlations are shown in Fig. 9, along with the correlating equations. The breakpoint between the lines is at $e^+ = 300$.

For the correlation of the Sherwood number results, a function H_e^+ is defined as

$$H_e^+ = [(f/8St) - 1]/(f/8)^{1/2} + R_e^+ \quad (13)$$

where

$$St = \overline{Sh}_{cyc}/Re\,Sc. \quad (14)$$

The $\overline{Sh}_{cyc}$, Re data were rephrased in terms of H_e^+ and e^+ and plotted in Fig. 10. The data are well correlated by these parameters, and a least-squares correlating equation is presented in the figure.

The highly satisfactory correlations in evidence in Figs. 9 and 10 encourage their use for interpolation between the present parameter values and for moderate extrapolation.

PERFORMANCE ASSESSMENTS

The fact that both the mass (heat) transfer coefficients and friction factors are increased by the presence of the periodic disturbance elements requires that further analysis be performed to assess the *net* effect of the disturbances. Such an assessment is usually made by comparing an enhanced configuration with a related baseline configuration. The comparison is carried out under a set of constraints which depend on the specifics of each application.

Here, the assessment methodology is illustrated by considering a flat rectangular duct of fixed cross-sectional and length dimensions. Three versions of the duct are to be compared: (1) no disturbance elements, (2) disturbance elements deployed along one principal wall, and (3) disturbance elements deployed along both principal walls. Among these, the disturbance-free duct will be regarded as the baseline case and is designated by an asterisk. The objective of the assessment is to determine which configuration has the highest fully developed mass (heat) transfer coefficient under the constraint that the pumping power be equal for all three configurations.

The pumping power PP is given by

$$PP = (\dot{w}/\rho)\Delta P \quad (15)$$

and the equal pumping power constraint can be expressed as

$$PP = (PP)^* \quad (16)$$

where the LHS refers to either of the enhanced (i.e. periodically disturbed) configurations while the RHS corresponds to the baseline case. For fixed duct dimensions and equal thermophysical properties, equation (16) becomes

$$f\,Re^3 = (f\,Re^3)^*. \quad (17)$$

Since the friction factor has been experimentally determined as a function of the Reynolds number for both the baseline and the enhanced configurations, equation (17) is a relation between Re and Re^*.

The numerical results obtained from the solution of equation (17) are presented in Fig. 11, where Re for the periodically disturbed configurations is plotted as a function of Re^* for the disturbance-free configuration. In each of the two graphs which make up Fig. 11, results are presented for six disturbed-duct cases. The $e/H = 0.082$ graph pertains to cases 1–3 of Table 1, with the suffix A denoting the two-sided disturbed duct and the suffix B denoting the one-sided disturbed duct. A similar set of results is conveyed in the $e/H = 0.164$ graph.

In general, for all cases depicted in Fig. 11, $Re < Re^*$. This finding is physically plausible since the higher pressure drops of the periodically disturbed ducts must be balanced by lower mass throughflows in order to satisfy the equal pumping power constraint. By the same reasoning, it follows that the higher pressure drops of the two-sided disturbed ducts (i.e. the A ducts) will yield lower Reynolds numbers than those for the one-sided disturbed ducts (B ducts). Also, since the pressure drop increases with decreasing pitch, it follows that the smaller the pitch. the lower the Reynolds number, so that the lines for cases 1–3 are arranged in ascending order (lowest pitch to highest pitch). Another relevant observation to be made in Fig. 11 is that the Re

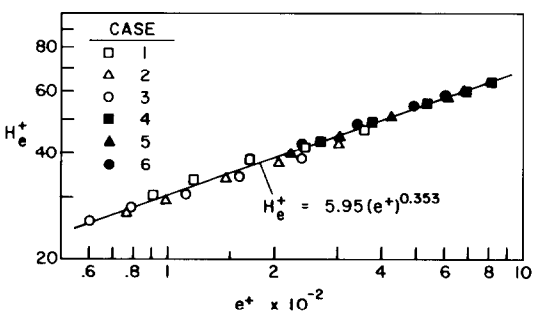

FIG. 10. Sherwood number correlation in terms of roughness parameters.

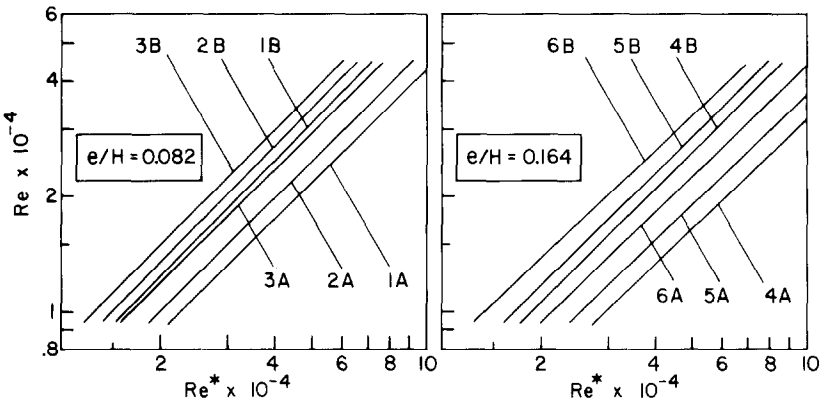

FIG. 11. Relationship between Re for periodically disturbed ducts and Re^* for a disturbance-free duct (equal pumping power constraint). The A curves are for two-sided disturbed ducts and the B curves are for one-sided disturbed ducts.

values for the $e/H = 0.164$ cases are lower than those for the $e/H = 0.082$ cases.

With the Re^*, Re information of Fig. 11, the corresponding Sherwood numbers can be evaluated and the ratio $(K/K^*)_{fd}$ determined, where the subscript fd denotes fully developed. Note that K_{fd} corresponds to Re and K^*_{fd} corresponds to Re^* (Re and Re^* are related according to Fig. 11). Furthermore, from the analogy between heat and mass transfer, $Nu/Pr^s = Sh/Sc^s$, so that

$$(K/K^*)_{fd} = (h/h^*)_{fd}. \tag{18}$$

The $(K/K^*)_{fd}$ results are plotted as a function of Re^* in Fig. 12. As in Fig. 11, there are two graphs, respectively for $e/H = 0.082$ and 0.164, with six disturbance-duct cases in each graph.

In assessing Fig. 12, the key issue is whether $(K/K^*)_{fd}$ is greater or less than one, with net enhancement corresponding to $(K/K^*)_{fd} > 1$. From the figure, it is seen that all of the $e/H = 0.082$ cases yield net enhancement. Over most of the Reynolds number range, the enhancement is greater for the two-sided disturbed ducts (A ducts) than for the one-sided disturbed ducts (B ducts), but at the higher end of the range the enhancements are about the same for the two types of ducts. For both ducts, the greatest enhancements occur at the lower Reynolds numbers and drop off as the Reynolds number increases, with a

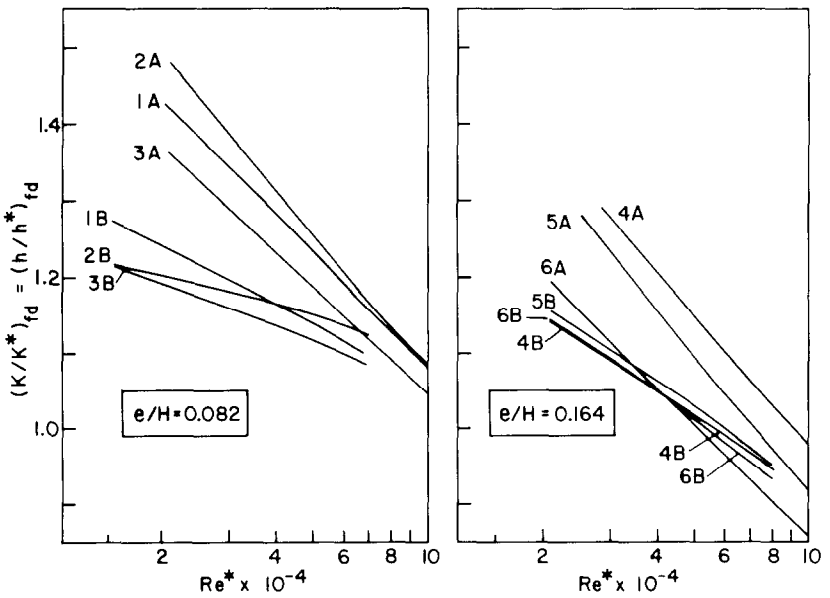

FIG. 12. Comparison of fully developed transfer coefficients for periodically disturbed ducts and a disturbance-free duct (equal pumping power constraint). The A curves are for two-sided disturbed ducts and the B curves are for one-sided disturbed ducts.

much more rapid dropoff for the two-sided disturbed duct. The maximum value of $(K/K^*)_{fd}$ for the $e/H = 0.082$ cases is just under 1.5, while the minimum value is about 1.1.

The $(K/K^*)_{fd}$ values for the $e/H = 0.164$ ducts are lower than those for the $e/H = 0.082$ ducts. Indeed, at the upper end of the Reynolds number range, $(K/K^*)_{fd} < 1$, indicating net degradation. The largest value of $(K/K^*)_{fd}$ for the $e/H = 0.164$ ducts is about 1.3.

The superior performance of the ducts with smaller e/H was already foretold by the Reynolds number results of Fig. 11, where it was noted that the equal-pumping-power Reynolds numbers for $e/H = 0.164$ were lower than those for 0.082.

The outcome of the performance assessment shows that there is merit to the use of periodic disturbances, provided that the geometrical parameters are selected with care.

CONCLUDING REMARKS

The present experiments have yielded both local and fully developed mass (heat) transfer coefficients for a flat rectangular duct having streamwise-periodic, two-dimensional disturbances at both of the principal walls. Fully developed friction factors were also determined. Three parameters were varied during the course of the investigation, including p/e (pitch-to-height ratio of the disturbance elements), e/H (ratio of disturbance height to duct height), and the Reynolds number Re. The results obtained here serve to complement and complete prior experimental results for a duct having disturbances at only one of the principal walls.

The local Sherwood number distributions revealed the rapid attainment of the periodic fully developed regime, and thereby underscored the importance of the fully developed mass (heat) transfer and friction results, whereby they became the main focus of the work.

The fully developed Sherwood numbers for a two-sided disturbed duct exceeded those for a one-sided disturbed duct, typically by about 40%. Relative to a disturbance-free duct, the presence of periodic disturbances at both principal walls yielded up to a three-fold increase in the Sherwood number at $Re = 10\,000$ and up to a 2.4-fold increase at $Re = 40\,000$.

The presence of disturbances at both walls also increased the fully developed friction factor relative to that for the one-sided disturbed duct. The increase was substantially greater for a duct of smaller height.

An analysis was carried out to assess the relative performances of the disturbance-free duct, the one-sided disturbed duct, and the two-sided disturbed duct. The analysis was performed for fixed duct dimensions and fixed pumping power and sought the largest values of the fully developed mass (heat) transfer coefficient. Relative to the disturbance-free duct, which served as a baseline case, the presence of periodic disturbances was found to be enhancing over a wide range of (but not all) conditions. For the most part, greater enhancement was attained with two-sided disturbances than with one-sided disturbances.

Compact correlations, suitable for interpolation and for moderate extrapolation, were developed for both the fully developed Sherwood number and friction factor. The correlation was achieved in terms of the so-called roughness parameters.

Acknowledgement—The research reported here was performed under the auspices of the Office of Naval Research.

REFERENCE

1. E. M. Sparrow and W. Q. Tao, Enhanced heat transfer in a flat rectangular duct with streamwise-periodic disturbances at one principal wall, *Trans. Am. Soc. Mech. Engrs*, Series C, *J. Heat Transfer* **105**, 851–861 (1983).

PERTURBATIONS SYMÉTRIQUES ET ASYMETRIQUES EN PAROI POUR UN ECOULEMENT CHAUFFE A SON PASSAGE

Résumé—On mesure les coefficients de transfert locaux et d'écoulement turbulent pleinement établi pour un canal rectangulaire ayant des perturbations périodiques dans le sens du courant, bidimensionnelles, et positionnées symétriquement sur les deux parois principales. On détermine aussi les facteurs de frottement. Les distributions du coefficient de transfert local montrent la rapide obtention du régime périodique établi. Les coefficients de transfert établis dépassent (de 40% environ) ceux pour un canal identique mais n'ayant des perturbations périodiques que sur une seule paroi principale (cas asymétrique). Les perturbations symétriques montrent aussi un accroissement significatif du transfert (jusqu'à un facteur trois) comparé au cas du canal sans perturbations. On observe aussi un grand accroissement du facteur de frottement. Une analyse basée sur des dimensions données du canal et une puissance de pompage fixée est conduite pour préciser la performance relative des canaux à perturbations symétriques et asymétriques et du canal libre. Pour un large domaine de conditions, le canal à perturbations symétriques possède les plus grands coefficients de transfert en fonction des paramètres de rugosité pour les coefficients de transfert thermique établi et pour les facteurs de frottement.

VERGLEICH VON SYMMETRISCHEN UND ASYMMETRISCHEN PERIODISCHEN STÖRUNGEN AN DEN WÄNDEN EINES BEHEIZTEN STRÖMUNGSKANALS

Zusammenfassung—In einem flachen Rechteck-Kanal mit zweidimensionalen, in Strömungsrichtung periodischen Störstellen, die symmetrisch an den Stirnseiten angeordnet sind, wurden durch Messungen Wärmeübergangskoeffizienten und Widerstandsbeiwerte bestimmt, und zwar die örtlichen und diejenigen in der vollausgebildeten turbulenten Strömung. Der Verlauf der örtlichen Übergangskoeffizienten zeigt, wie rasch sich der periodisch-vollausgebildete Zustand einstellt. Die Übergangskoeffizienten bei vollausgebildeter Strömung übertreffen diejenigen (typischerweise um 40%), die sich in einem Kanal ergeben, der bei sonst gleichen Voraussetzungen an nur einer Stirnseite periodische Störungen aufweist (asymmetrischer Fall). Die symmetrischen Störstellen führen im Vergleich zu einem entsprechenden störungsfreien Kanal ebenfalls zu wesentlich erhöhten Übertragungskoeffizienten (bis zum Faktor drei). Ebenso verursachen die Störungen ein starkes Ansteigen des Widerstandsbeiwertes. Bei konstanten Werten für die Kanalabmessungen und die Pumpenleistung wurde das relative Verhalten des symmetrisch gestörten, des asymmetrisch gestörten und des ungestörten Kanals abgeschätzt. Für einen großen Betriebsbereich ergaben sich die größten Übergangskoeffizienten (bei vollausgebildeter Strömung) im symmetrisch gestörten Kanal. Für die Wärmeübergangskoeffizienten und die Widerstandsbeiwerte bei vollausgebildeter Strömung werden in Abhängigkeit von Rauhigkeitsparametern kompakte Korrelationen gebildet.

СРАВНЕНИЕ СИММЕТРИЧНЫХ И НЕСИММЕТРИЧНЫХ ПЕРИОДИЧЕСКИХ ВОЗМУЩЕНИЙ НА СТЕНКАХ НАГРЕВАЕМОГО ТРУБОПРОВОДА

Аннотация—Проведены измерения коэффициентов локального теплопереноса и коэффициентов трения для полностью развитого турбулентного течения в плоском прямоугольном канале с периодическими по течению двумерными возмущениями, симметричными по отношению к двум основным стенкам. Распределения коэффициента локального теплопереноса выявили быстрое установление периодического полностью развитого режима. Значения коэффициентов для полностью развитого теплопереноса превышали (обычно на 40%) соответствующие коэффициенты для идентичного трубопровода с периодическими возмущениями только у одной из основных стенок (несимметричный случай). Симметричные возмущения также приводили к существенному росту коэффициентов теплопереноса (в три раза) по сравнению с коэффициентами в соответствующих трубопроводах без возмущений. Также наблюдался большой рост коэффициента трения за счет возмущений. Для оценки относительных характеристик трубопроводов с симметричными и несимметричными возмущениями и без возмущений проведен анализ для заданных размеров трубопровода и расхода энергии на привод насоса. В широком диапазоне условий в трубопроводе с симметричными возмущениями получены самые большие значения коэффициентов для полностью развитого теплопереноса. Как для коэффициентов полностью развитого теплопереноса, так и для коэффициентов трения выведены простые соотношения, выраженные через параметры шероховатости.